

## Bioorthogonal “Labeling after Recognition” Affording an FRET-based Luminescent Probe for Detecting and Imaging Caspase-3 via Photoluminescence Lifetime Imaging

Qi Wu, Kenneth Yin Zhang, Peiling Dai, Hengyu Zhu, Yun Wang, Linna Song, Ling Wang, Shujuan Liu, Qiang Zhao, and Wei Huang

*J. Am. Chem. Soc.*, **Just Accepted Manuscript** • DOI: 10.1021/jacs.9b12191 • Publication Date (Web): 17 Dec 2019

Downloaded from [pubs.acs.org](https://pubs.acs.org) on December 18, 2019

### Just Accepted

“Just Accepted” manuscripts have been peer-reviewed and accepted for publication. They are posted online prior to technical editing, formatting for publication and author proofing. The American Chemical Society provides “Just Accepted” as a service to the research community to expedite the dissemination of scientific material as soon as possible after acceptance. “Just Accepted” manuscripts appear in full in PDF format accompanied by an HTML abstract. “Just Accepted” manuscripts have been fully peer reviewed, but should not be considered the official version of record. They are citable by the Digital Object Identifier (DOI®). “Just Accepted” is an optional service offered to authors. Therefore, the “Just Accepted” Web site may not include all articles that will be published in the journal. After a manuscript is technically edited and formatted, it will be removed from the “Just Accepted” Web site and published as an ASAP article. Note that technical editing may introduce minor changes to the manuscript text and/or graphics which could affect content, and all legal disclaimers and ethical guidelines that apply to the journal pertain. ACS cannot be held responsible for errors or consequences arising from the use of information contained in these “Just Accepted” manuscripts.

# Bioorthogonal “Labeling after Recognition” Affording an FRET-based Luminescent Probe for Detecting and Imaging Caspase-3 via Photoluminescence Lifetime Imaging

Qi Wu,<sup>†</sup> Kenneth Yin Zhang,<sup>\*,†</sup> Peiling Dai,<sup>†</sup> Hengyu Zhu,<sup>†</sup> Yun Wang,<sup>†</sup> Linna Song,<sup>†</sup> Ling Wang,<sup>†</sup> Shujuan Liu,<sup>†</sup> Qiang Zhao,<sup>\*,†</sup> and Wei Huang<sup>\*,†,‡</sup>

<sup>†</sup> Key Laboratory for Organic Electronics and Information Displays & Jiangsu Key Laboratory for Biosensors, Institute of Advanced Materials (IAM), Jiangsu National Synergetic Innovation Center for Advanced Materials (SICAM), Nanjing University of Posts & Telecommunications, 9 Wenyuan Road, Nanjing 210023, P. R. China

<sup>‡</sup> Xi'an Institute of Flexible Electronics (XIFE), Northwestern Polytechnical University (NPU), 127 West Youyi Road, Xi'an 710072, P. R. China

**ABSTRACT:** Bis-labeling with luminescent energy donor/acceptor pair onto biological substrates affords probes which give FRET readouts for detection of interaction partners. However, the covalently bound luminophores bring about steric hindrance and non-specific interaction, which probably perturb the biological recognition. Herein, we designed a highly sensitive and specific “labeling after recognition” sensing approach, where luminophore labeling occurred after the biological recognition. Taking the cutting enzyme caspase-3 as an example, we demonstrated the detection of its catalytic activity in solution and apoptotic cells using the tetrapeptide motif Asp-Glu-Val-Asp (DEVD) as the cleavable substrate, and an iridium(III) complex and a rhodamine derivative as the energy donor/acceptor pair. The DEVD tetrapeptide was modified with an azide and a GK-norbornylene groups at the amino and carboxyl terminuses, respectively, which allowed donor/acceptor bis-labeling via two independent catalysis-free bioorthogonal reactions. The phosphorescence lifetime of the iridium(III) complex was quenched upon bis-labeling owing to the intracellular FRET to the rhodamine derivative, and significantly elongated upon the peptide was catalytically cleaved by caspase-3. Interestingly, the sensitivity and efficiency of the lifetime response were much higher in the “labeling after recognition” sensing approach. Molecular docking analysis showed that the steric hindrance and non-specific interactions partially inhibited the biological recognition of the DEVD substrate by caspase-3. The imaging of the catalytic activity of caspase-3 in apoptotic cells was demonstrated via photoluminescence lifetime imaging microscopy (PLIM). Lifetime analysis not only confirmed the occurrence of intracellular bioorthogonal bis-labeling and catalytic cleavage, but also showed the extent to which the two dynamic processes occurred.

## INTRODUCTION

Fluorescence resonance energy transfer (FRET)-based probes involving two luminophores as an energy donor/acceptor pair have been widely designed for sensing different intracellular biomolecules.<sup>1-4</sup> Upon interaction with specific biomolecules, the proximity and orientation of the donor/acceptor pair determine the FRET luminescence readout. Many examples demonstrated bis(luminophore)-labeled probes for bioimaging of molecular analytes such as pH values,<sup>5</sup> metal ions,<sup>6,7</sup> and biosulfides,<sup>8,9</sup> and biological parameters<sup>10</sup> and activities.<sup>11-13</sup> Cutting enzymes that are able to cleave the linkage between the donor/acceptor pair are possible ideal targets of FRET probes because the readout luminescence is changed to the maximum extent. However, the utilization of FRET probes for enzyme detection is relatively rare compared to sensing for other small molecular analytes.<sup>14</sup> Given that there are a variety of fluorescent and phosphorescent probes and imaging reagents available for selection as donor/acceptor pairs, the

main limitations are difficulty in synthesis and reduced catalytic activity of enzymes in the presence of two luminophores.

As illustrated in Figure 1, traditional FRET sensing of cutting enzymes is a “labeling before recognition” process.<sup>13,14</sup> The recognition substrate serves as a linker and is first labeled with two luminophores as a donor/acceptor pair at the two ends. Upon recognition by a specific enzyme, the substrate is catalytically cleaved and the two luminophores are separated, leading to remarkable FRET readout. However, the bulky luminophores probably increase the steric hindrance disturbing specific enzyme recognition or induce non-specific affinity toward other biomolecules, especially in a complex intracellular environment. To address these problems, in this work we designed a new “labeling after recognition” sensory strategy by using bioorthogonal labeling technique, which has been widely used to label intracellular biomolecules in their native environments,<sup>15,16</sup> but has not been used to generate an intracellular probe for biosensing. Instead of luminophores,

two chemical reporters are incorporated into the recognition substrate. The chemical reporters are small, non-native, and non-perturbing chemical functionality,<sup>15,16</sup> which can be sensitively recognized by exogenously delivered luminophores. Since the bioorthogonal labeling of luminophores occurs after the catalytic cleavage by the cutting enzyme, steric hindrance or non-specific interaction is minimized and high specificity and sensitivity are anticipated.

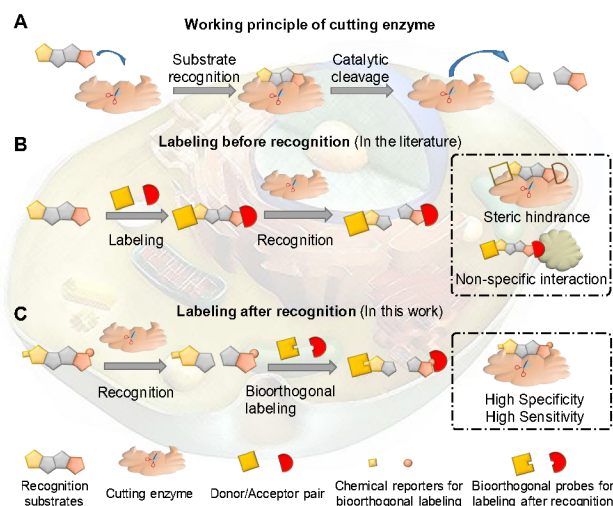


**Figure 1.** (A) Schematic representation of the recognition and catalytic cleavage of a substrate by a specific cutting enzyme. (B) Schematic representation of FRET-based sensing of cutting enzymes via a “labeling before recognition” process in the literature. (C) Schematic representation of FRET-based sensing of cutting enzymes via a “labeling after recognition” process in this work.

A new challenge is to select suitable donor/acceptor pairs and bioorthogonal reactions to realize wash-free real-time imaging in living cells. There are some requirements to be fulfilled. First, a large wavelength overlap between the emission of donor and the absorption of acceptor favors the occurrence of FRET.<sup>17</sup> Second, there is no crosstalk between two bioorthogonal reactions for donor and acceptor labeling.<sup>18,19</sup> Third, for both donor and acceptor, the labeled luminophore is easily distinguishable from the unlabeled one to minimize possible interference from free luminophores during imaging. Luminophores with emission turn-on upon bioorthogonal labeling are attractive, but fluorogenic probes available for use are very limited.<sup>20,21</sup> Luminophores with variation in emission lifetimes are also potential candidates.<sup>22,23</sup> The labeled luminophore is readily differentiated from unlabeled one via photoluminescence lifetime imaging microscopy (PLIM). Additionally, the lifetime of the donor is also a sensitive variable depending on the donor/acceptor distance in FRET sensing.<sup>24</sup> Whereas intensity analysis shows overall brightness over a certain range of wavelength, lifetime imaging explicitly gives different lifetime values for analytes on different states with high spatial resolution quantitatively and summarizes the occurrence of every state. Furthermore, the lifetime value is sensitive to the molecular structure but independent of the concentration, which is promising for eliminating interference from dynamic concentration variation during imaging in living cells.<sup>25</sup>

Caspase-3 is an important cutting enzyme which is activated in early apoptosis and catalyzes the cleavage of the

tetrapeptide motif Asp-Glu-Val-Asp (DEVD).<sup>26</sup> In view of the important biological roles of caspase-3, in this study we took it as an example to demonstrate our proposed “labeling after recognition” sensing. The tetrapeptide DEVD was modified with an azide and a norbornylene groups as two chemical reporters at the amino and carboxyl terminuses, respectively. A phosphorescent iridium(III) complex functionalized with dibenzocyclooctyne<sup>27-31</sup> and a rhodamine derivative modified with a tetrazine unit<sup>32</sup> were chosen as the donor and the acceptor, respectively. Their bioorthogonal labeling behavior and photophysical response toward labeling have been investigated using azido acetic acid and 5-norbornene-2-methylamine as model substrates. When the donor/acceptor pair were labeled onto the same peptide molecule, intramolecular FRET occurred and the phosphorescence lifetime of the iridium(III) complex was shortened. Once the peptide was cleaved by caspase-3, the phosphorescence lifetime was recovered, indicating that the lifetime value could be used as an indicator for measuring the catalytic activity of caspase-3. Interestingly, the lifetime response in the “labeling after recognition” sensing was much faster and more significant compared to that in the widely-used “labeling before recognition” sensing. Molecular modeling study confirmed that labeling with two luminophores brought about steric hindrance and nonspecific interactions, and increased the free binding energy of the peptide and caspase-3. Detection of the catalytic activity of caspase-3 during cellular apoptosis has also been demonstrated using the “labeling after recognition” approach via photoluminescence lifetime imaging. Compared to intensity-based imaging, lifetime analysis gave detail visualization of intracellular caspase-3 induced peptide cleavage with spatial resolution.

## RESULTS AND DISCUSSION

A phosphorescent iridium(III) complex (**1**) and a rhodamine derivative (**2**) were used as the donor and the acceptor, respectively (Figure 2A, 2B). Their synthesis (Figure S1, S2) and characterization by <sup>1</sup>H and <sup>13</sup>C nuclear magnetic resonance (NMR) and matrix-assisted laser desorption ionization time-of-flight (MALDI-TOF) mass spectrometer (MS) were shown in supporting information. Selection of an iridium(III) complex as the energy donor is because the long-lived phosphorescence is distinguishable from short-lived autofluorescence via PLIM<sup>25</sup> and the lifetime is highly sensitive to structure modification such as bioorthogonal labeling.<sup>22</sup> The iridium(III) complex **1** was functionalized with dibenzocyclooctyne (DIBO), which readily undergoes strain-promoted alkyne-azide cycloaddition (SPAAC) without catalysis (Figure 2A).<sup>27-31</sup> The rhodamine derivative **2** was modified with a tetrazine unit which is expected to quench the fluorescence and enable the turn-on response toward inverse-electron demand Diels-Alder cycloaddition (iEDDAC) with dienophiles such as norbornylene (Figure 2B).<sup>32</sup> Additionally, the phosphorescence spectrum of complex **1** was well overlapped with the absorption spectrum of compound **2** (Figure S3), ensuring efficient intramolecular FRET when they were labeled onto the same species. Furthermore, the two bioorthogonal labeling processes are supposed to be independent of each other.

The labeling behavior of **1** and **2** and their photophysical response toward their corresponding labeling reactions was investigated using azido acetic acid (**1a**) and 5-norbornene-2-

methylamine (**2a**) as model substrates, respectively. Formation of the resultant compounds **1b** and **2b** in 5 min was confirmed by the MALDI-TOF MS analysis (Figure 2C, 2D), though they were obtained as a mixture of regioisomers. The MS spectrum of a mixture of **1**, **2**, **1a**, and **2a** revealed four peaks at  $m/z = 625$ , 721, 1046, and 1147, corresponding to **2**, **2b**, **1**, and **1b**, respectively (Figure 2E), demonstrating no crosstalk between the two labeling reactions.

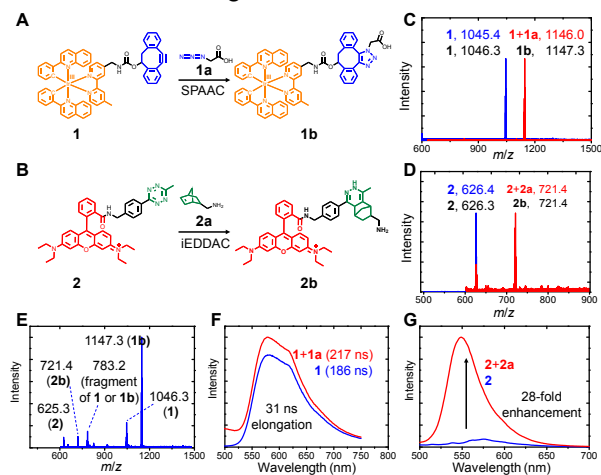


**Figure 2.** (A) SPAAC bioorthogonal labeling reaction of complex **1** and **1a** to yield **1b**. (B) iEDDAC bioorthogonal labeling reaction of compound **2** and **2a** to yield **2b**. The MALDI-TOF MS spectra of a mixture of **1** and **1b** (C), **2** and **2b** (D), and **1**, **1a**, **2**, and **2a** (E). Luminescence spectra of complex **1** and a mixture of **1** and **1a** (F), and compound **2** and a mixture of **2** and **2a** (G) in DMSO/PBS buffer (1 : 99, v/v, pH = 7.4) at room temperature.

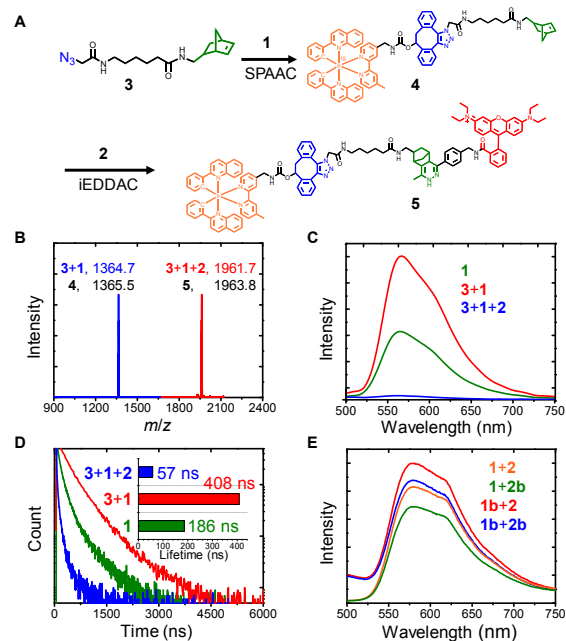


**Figure 3.** (A) Bioorthogonal labeling reactions yielding compounds **4** and **5**. (B) The MALDI-TOF MS spectra of a mixture of **1** and **3** before (blue) and after (red) addition of **2**. The calculated masses of **4** and **5** are shown in black for comparison. Luminescence spectra (C) decay curves (D) and lifetime values (insets in (D)) of **1** and resultant conjugates upon each step of labeling in DMSO/PBS buffer (1 : 99, v/v, pH = 7.4) at room

temperature. (E) Luminescence spectra of pairwise mixtures under the same condition.

Accompanying the SPAAC labeling, complex **1** exhibited reduced absorption at 270 – 310 nm (Figure S4), which has also been observed upon addition of **1a** to 4-dibenzocyclooctynol. Upon photoexcitation, complex **1** exhibited intense luminescence at 573 nm with a lifetime of 186 ns in phosphate buffer saline (PBS) buffer at pH 7.4. The phosphorescence was slightly enhanced by 1.2 fold upon addition of **1a**, but the spectrum was indistinguishable from that of complex **1** (Figure 2F). Compound **2** exhibited the absorption maximum at about 537 nm and was nonemissive in solution owing to the efficient quenching by the tetrazine moiety. Intense fluorescence was turned on upon generating **2b** with an enhancement factor of 28 fold (Figure 2G and Figure S5). Thus, intracellular labeling of the acceptor is readily visualized via laser-scanning fluorescence confocal microscopy. To investigate the effect of intramolecular FRET on the phosphorescence properties of the donor, **1** and **2** were allowed to react with the azide-C6-norbornene model compound **3** to yield **4** and **5** in two steps (Figure 3A). The MS spectra of the resultant conjugates in each step were shown in Figure 3B, confirming the generation of **4** and **5**. After the SPAAC labeling of complex **1**, the phosphorescence of **1** was enhanced by 2.1 fold with the lifetime elongated to 408 ns (Figure 3C and 3D), which was significantly quenched with the lifetime shortened to 57 ns upon further iEDDAC tetrazine-norbornene click reaction with compound **2**, indicative of efficient intramolecular FRET from iridium(III) to rhodamine. According to the equation ( $E = 1 - \tau_{D_A}/\tau_D$ ), the FRET efficiency ( $E$ ) in compound **5** was calculated to be 86%. For comparison, the phosphorescence spectra of the pairwise mixtures of **1** and **2**, **1** and **2b**, **1b** and **2**, and **1b** and **2b** were recorded and shown in Figure 3E to evaluate the intermolecular energy transfers. These mixtures maintained the luminescence characteristics of complex **1** or **1b** with the lifetimes longer than 180 ns.

The utilization of **1** and **2** as a donor/acceptor pair for detection of caspase-3 was demonstrated in PBS buffer containing 1% dimethyl sulfoxide (DMSO) and 10% fetal bovine serum (FBS) using DEVD tetrapeptide as the cleavable substrate. The presence of FBS (10%) helped to maintain the polarity and viscosity of the solution unchanged upon addition a small amount of caspase-3. The tetrapeptide DEVD modified with an azide and a GK-norbornylene groups at the amino and carboxyl terminuses, respectively (Figure 4A), ( $N_3$ -DEVDGK-norbornylene) was purchased from ChinaPeptides. In the typical “labeling before recognition” sensing (Figure 4B), the peptide was first labeled with **1** and **2**. Upon addition of the stock mixture of **1** (10  $\mu$ M) and **2** (10  $\mu$ M) to  $N_3$ -DEVDGK-norbornylene (10  $\mu$ M), successful and efficient bis-bioorthogonal labeling (Figure 4A) in less than 0.5 h was confirmed by the observation that the fluorescence of compound **2** was turned on (Figure S6) and the phosphorescence lifetime of complex **1** was shortened from 1389 to 1023 ns. The FRET efficiency in the **1**-peptide-**2** conjugate was calculated to be 26%, which was much smaller than that in compound **5**, because the peptide linker was much longer than the spacer-arm **3**, leading to a longer distance between the two luminophores. Addition of caspase-3 (50 pM) to the **1**-peptide-**2** conjugate gradually elongated the lifetime to 1299 ns in 2 h at 37  $^{\circ}$ C. In another experiment, which we

call “labeling after recognition”, the caspase-3 (50 pM) was first added to the cleavable peptide (10  $\mu$ M) and the mixture was stirred gently at 37  $^{\circ}$ C for 0.5 – 2 h (Figure 4C). The stock mixture of **1** (10  $\mu$ M) and **2** (10  $\mu$ M) was added for labeling 0.5 h before lifetime measurement. As shown in Figure 4D, increasing the duration of the recognition resulted in a longer phosphorescence lifetime. Two control experiments were performed where the caspase-3 enzyme or the peptide was absent. In the absence of caspase-3, the **1**-peptide-**2** conjugate kept the lifetime of about 1023 ns at 37  $^{\circ}$ C almost unchanged (Figure 4D). In the absence of the peptide, the mixture of **1**, **2** and caspase-3 exhibited a phosphorescence lifetime of about 1395 ns. The lifetime elongation in the two sensing experiments indicated that the intramolecular FRET was inhibited owing to the catalytic cleavage of the peptide by caspase-3. Thus, the phosphorescence lifetime can be used as

an indicator of the catalytic activity of caspase-3. Interestingly and importantly, the lifetime response in the “labeling after recognition” sensing was much faster and more significant compared to that in the “labeling before recognition” sensing. The lifetime reached an equilibrium point in 1.5 h and the lifetime value was comparable to that in the control experiment where the peptide was absent. Further increasing recognition time did not elongate the lifetime much. These results suggested that the peptide was almost completely cleaved in 1.5 h and indicated that “labeling after recognition” was much more sensitive and more efficient than “labeling before recognition” in the detection of caspase-3. Such difference has been tentatively ascribed to that luminophore-induced steric hindrance and/or non-specific interaction was avoided during catalytic cleavage in the “labeling after recognition” approach.

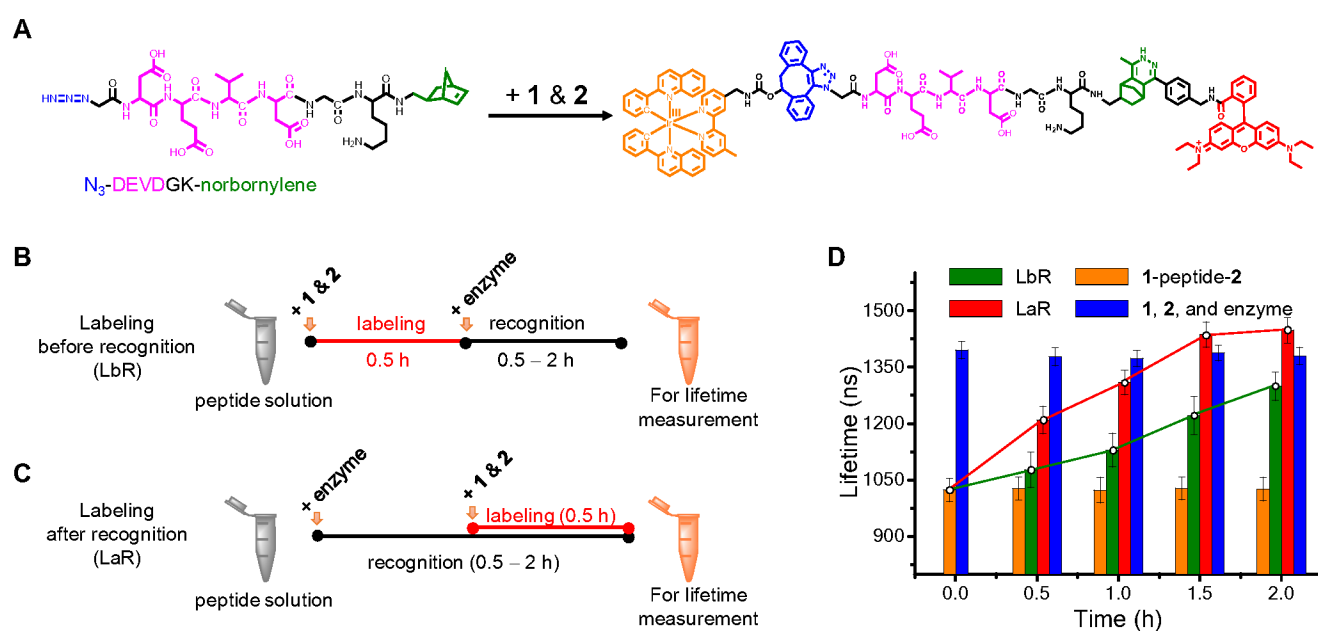


**Figure 4.** (A) The chemical structures of  $N_3$ -DEVDGK-norbornylene and the bioorthogonal labeling reaction with **1** and **2**. Scheme showing the caspase-3 detection in the “labeling before recognition” approach (B) and the “labeling after recognition” approach (C). (D) Phosphorescence lifetime traces upon caspase-3–DEVD recognition for 0.5 – 2 h in two sensing approaches. Error bars represent the standard deviations of three independent measurements.

To gain insight into the possible binding mode on the DEVD binding site of caspase-3 and the structural basis underlying the differences in the sensitivity of the two sensing approaches, molecular docking<sup>23–35</sup> was performed for the azide and norbornylene bis-modified peptide before and after bis-bioorthogonal labeling. The coordinates of the protein structure of caspase-3–DEVD were obtained from the Protein Data Bank (PDB code: 3PD0)<sup>36</sup> and the model substrate AC-DEVD-CMK (Figure 5A) was extracted via PyMOL. Molecular docking of the DEVD-containing peptide into caspase-3 was achieved in AutoDock 4.2.<sup>37,38</sup> As shown in Figure 5B, the model substrate was buried in the pocket forming hydrogen bonds with Phe-250, Asn-208, Arg-207, Ser-205, Gln-161, Arg-64 residues of caspase-3. The bond lengths ranged from 2.07 to 3.47 Å. Modification of the tetrapeptide motif with azide and norbornylene groups did not remarkably affect the binding to caspase-3.  $N_3$ -DEVDGK-norbornylene located in the same pocket and hydrogen bonds

with the same residues were also present (Figure 5C). The coordinates of  $N_3$ -DEVDGK-norbornylene were quite similar to those of the model substrate AC-DEVD-CMK (Figure 5D) and the free binding energy was calculated to be  $-8.08$  kcal/mol (Figure 5E) which was slightly higher than that of AC-DEVD-CMK ( $-8.21$  kcal/mol). After bioorthogonal labeling, upon docking **1**-DEVDGK-**2** into the same pocket, similar hydrogen bonds were not observed except those with Arg-207 and Ser-205 residues (Figure 5F) and the free binding energy increased to  $-4.12$  kcal/mol probably due to steric hindrance caused by the large molecular sizes of complex **1** and compound **2**. The coordinates of **1**-DEVDGK-**2** were very different from those of the model substrate AC-DEVD-CMK (Figure 5G). Additional interactions with Ser-65, Thr-62, Ser-209, Arg-164 residues were observed (Figure 5F), which may lead to non-specific affinity during DEVD recognition by caspase-3. Taken together, the results of molecular docking studies showed that  $N_3$ -DEVDGK-norbornylene was more

easily recognized by caspase-3 before luminophore labeling compared to **1**-DEVDGK-**2**, which also well explained why the “labeling after recognition” sensing of caspase-3 exhibited a higher sensitivity compared to the “labeling before recognition” sensing.

Intracellular bioorthogonal labeling has been investigated via confocal luminescence and lifetime imaging microscopy. Both **1** and **2** showed negligible cytotoxic effect toward living HeLa cells under the imaging conditions as revealed by the 3-(4,5-dimethyl-2-thiazolyl)-2,5-diphenyltetrazolium bromide (MTT) assay (Figure S7). HeLa cells incubated with complex **1**

(5  $\mu$ M, 30 min) exhibited intense intracellular luminescence (Figure S8A). Further incubation with **1a** (5  $\mu$ M, 30 min) did not cause remarkable change in the staining pattern or emission intensity. Decay analysis of the intracellular luminescence via PLIM indicated an elongation of the emission lifetime from about 665 ns to 683 ns upon intracellular SPAAC forming **1b** (Figure S8A). In another experiment, HeLa cells incubated with compound **2** (5  $\mu$ M, 30 min) remained nonemissive under photoexcitation at 515 nm until further loading of **2a** (5  $\mu$ M, 30 min) to activate iEDDAC labeling and generate fluorescent **2b** (Figure S8B).

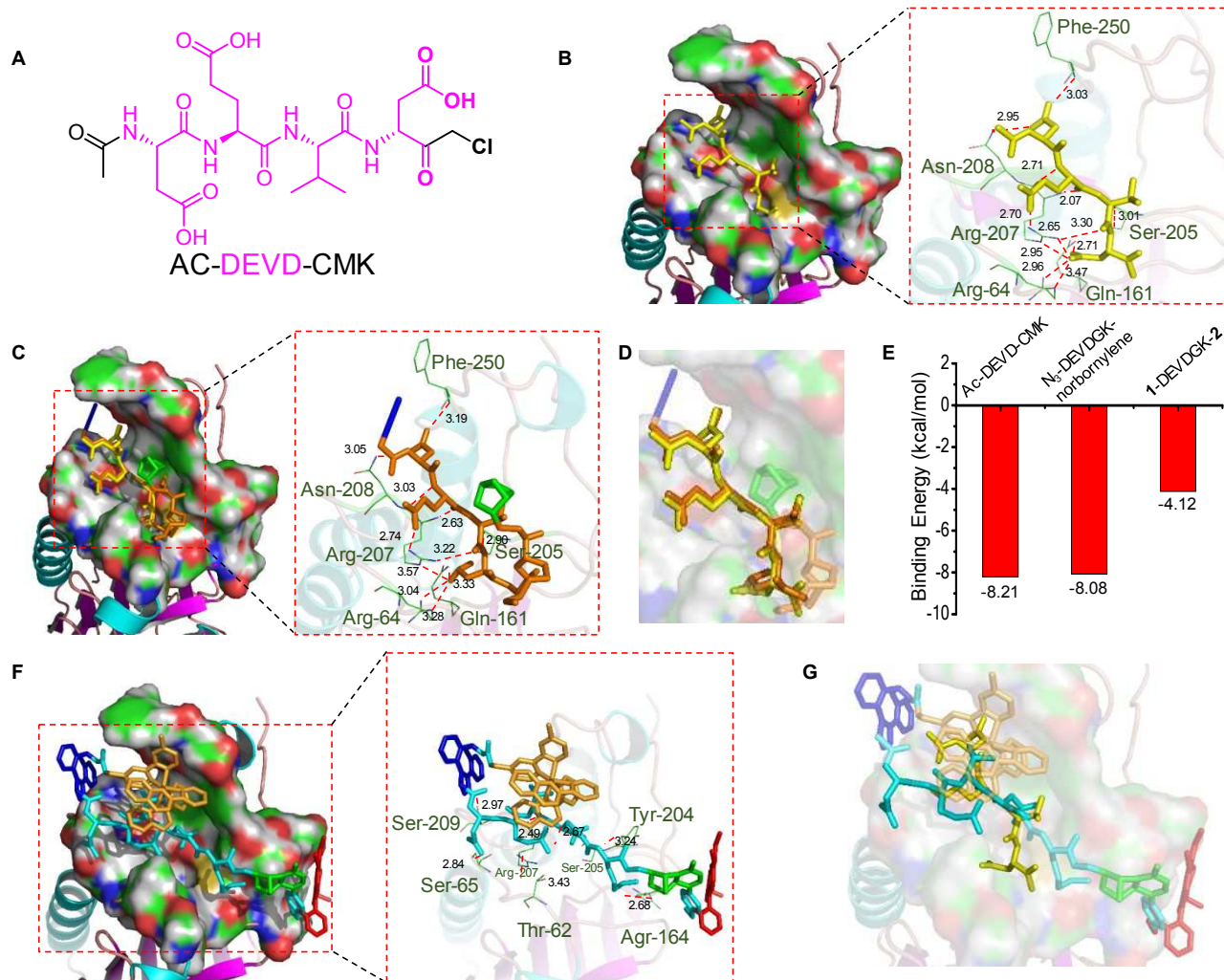


**Figure 5.** (A) The chemical structure of the model substrate of caspase-3, AC-DEVD-CMK. Binding pocket and conformation of AC-DEVD-CMK (B) and N<sub>3</sub>-DEVDGK-norbornylene (C) in caspase-3. The hydrogen-bond interactions and bond-lengths (Å) with key amino acid residues in the binding site are shown. (D) Overlap view of AC-DEVD-CMK and N<sub>3</sub>-DEVDGK-norbornylene in the binding pocket of caspase-3. The DEVD segment was yellow and orange in AC-DEVD-CMK and N<sub>3</sub>-DEVDGK-norbornylene, respectively. (E) Calculated free binding energy of AC-DEVD-CMK, N<sub>3</sub>-DEVDGK-norbornylene, and **1**-DEVDGK-**2** toward caspase-3. (F) Binding pocket and conformation of **1**-DEVDGK-**2** in caspase-3. (G) Overlap view of AC-DEVD-CMK and **1**-DEVDGK-**2** in the binding pocket of caspase-3. The DEVD segment was yellow and sky-blue in AC-DEVD-CMK and **1**-DEVDGK-**2**, respectively.

Then we demonstrated the simultaneous labeling of **1** and **2** onto N<sub>3</sub>-DEVDGK-norbornylene in living cells. HeLa cells were first simultaneously incubated with **1** (5  $\mu$ M) and **2** (5  $\mu$ M) for 30 min followed by incubation with N<sub>3</sub>-DEVDGK-norbornylene. Photoluminescence confocal imaging revealed moderate emission quenching upon bis-labeling (Figure S9). The phosphorescence lifetime of complex **1** at  $575 \pm 25$  nm was recorded via PLIM. As shown in Figure 6A, before

bioorthogonal labeling, intracellular complex **1** exhibited a lifetime of about 660 ns and the lifetime distribution inside the cells was even. Upon incubation with N<sub>3</sub>-DEVDGK-norbornylene for 10 min, some short-lived spots appeared inside the cells (Figure 6B,C). The lifetime values of the long-lived and short-lived spots were determined to be 672 ns and 533 ns, respectively, giving an averaged lifetime of 627 ns (Figure 6D). The short-lived spots have been assigned to bis-

labeled peptide and the long-lived signals originated from free complex **1** or monolabeled **1**-peptide conjugate, respectively. As incubation proceeded, the short-lived spots became dominant, indicating more peptide molecules were bis-labeled. The averaged lifetime reached the shortest value of 513 ns in 50 min and the lifetime distribution returned to uniformity, indicating that the labeling was successful and finished. Analysis of the relative occurrence of the long-lived and short-lived signals gave an approximate overview on the degree of bis-labeling occurred. About 83.5% of intracellular complex **1** appeared on the bis-labeled peptide in 50 min of peptide incubation (Figure 6E). The fluorescence of compound **2** was turned on upon labeling and the fluorescence pattern exhibited a good colocalization coefficient (91%) with the phosphorescence of complex **1** (Figure S10A), suggesting that **1** and **2** were labeled onto the same peptide molecule inside the cells. When **1a** and **2a** were used for intracellular bioorthogonal labeling instead of  $N_3$ -DEVDGK-norbornylene, similar fluorescence turn-on of compound **2** was observed, but the colocalization coefficient dropped to 25% (Figure S10B). This is because **1** and **2** were labeled on different molecules, although the labeling reactions occurred.

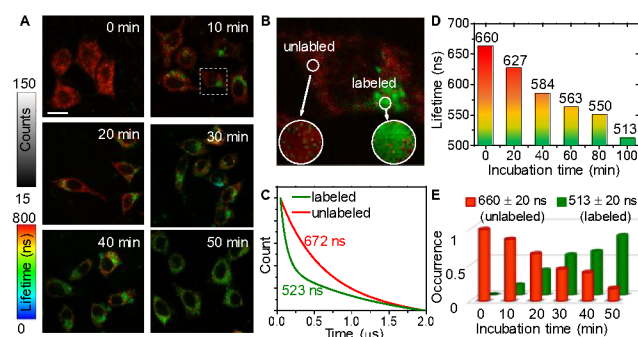


**Figure 6.** (A) Photoluminescence lifetime confocal microscopy images of living HeLa cells preloaded with **1** and **2** and then incubated with  $N_3$ -DEVDGK-norbornylene (5  $\mu$ M) for 0 – 50 min. Enlarged view of the marked area in (A). (C) The photoluminescence decay curves of the circled area in (B). (D) Averaged lifetime values of living HeLa cells preloaded with **1** and **2** and then incubated with  $N_3$ -DEVDGK-norbornylene (5  $\mu$ M) for 0 – 50 min. (E) Relative occurrence of long-lived and short-lived signals during lifetime imaging. Scale bar: 20  $\mu$ m.

The catalytic activity of intracellular caspase-3 during cellular apoptosis was measured via PLIM. In the “labeling before recognition” approach, conjugate **1**-DEVDGK-**2** was first prepared extracellularly in solution and then added into the medium for cellular uptake. However, the internalization of this conjugate was inefficient and insufficient photon signals were detected during PLIM analysis. Using bioorthogonal probes to form the conjugate intracellularly perfectly solved this problem. HeLa cells were first incubated with  $N_3$ -DEVDGK-norbornylene and then complex **1** and compound **2** were added into the culture medium for intracellular bioorthogonal labeling. After that, cisplatin was used to induce cellular apoptosis<sup>39,40</sup> and the phosphorescence lifetime was measured in 4 h. In the “labeling after recognition” experiment, cells were incubated with  $N_3$ -DEVDGK-norbornylene and then stimulated with cisplatin for 4 h. Complex **1** and compound **2** were added into the culture medium 1 h before photoluminescence lifetime imaging. The luminescence images were shown in Figure S11. The intensity

response was not significant in either sensing approach. As shown in the PLIM images (Figure 7A), in both sensing approaches, the intracellular phosphorescence lifetime became longer when the cells were stimulated with cisplatin, indicating that caspase-3 was activated when the cells initiated apoptosis. Lifetime analysis showed that as the concentration of cisplatin increased, the long lifetime spots became more and the short lifetime spots became fewer in the PLIM images (Figure 7B), resulting in elongation of the averaged lifetime values (Figure 7C). The relative occurrence of the long-lived signals in the lifetime images reflected the extent to which the catalytic cleavage proceeded. Colocalization analysis of the phosphorescence of complex **1** and the fluorescence of compound **2** showed that the coefficients dropped from about 90% to about 20% when the cells were treated with 40  $\mu$ g/mL of cisplatin for 4 h (Figure S12A), which confirmed that the peptide was catalytically cleaved by activated caspase-3 during cellular apoptosis. As in the case of sensing in solution, the lifetime response toward activated caspase-3 in apoptotic cells is faster and more sensitive during “labeling after recognition” imaging compared to “labeling before recognition” sensing. Especially, when the cells were treated with cisplatin at a concentration as low as 1  $\mu$ g/mL, the lifetime of conjugate **1**-DEVDGK-**2** was hardly responsive in 4 h, but in contrast, long-lived spots with a lifetime of about 670 ns were observed (Figure 7D) and accounted for about 32% of the emissive spots when labeling took place after the catalytic peptide cleavage, which led to an increase of the averaged lifetime to about 556 ns. When increasing the duration of cisplatin treatment to 24 h, the difference in the lifetimes measured in the two sensing approaches was not that big (Figure S12B), indicating that the cleavage products was the same during the two sensing approach, but the lifetime response in the “labeling after recognition” was much faster.

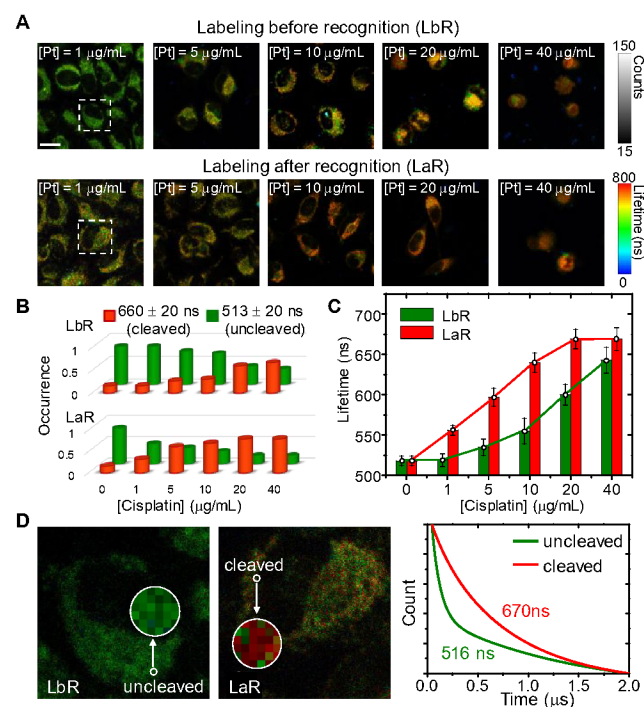


**Figure 7.** (A) Photoluminescence lifetime confocal microscopy images of HeLa cells stimulated with cisplatin at different concentrations for 4 h in two different sensing approaches. (B)

Relative occurrence of long-lived and short-lived signals during lifetime imaging. (C) Averaged lifetime values of the lifetime images. Error bars represent the standard deviations of three independent measurements. (D) Enlarged view of the marked area in (A) and photoluminescence decay curves of the circled area. Scale bar: 20  $\mu\text{m}$ .

## CONCLUSION

Labeling of substrate with luminescent tags has been extensively used for signaling and imaging of a variety of biomolecules owing to the specific and strong substrate-biomolecule interactions. Bis-labeling of an energy donor and acceptor facilitates FRET-based signaling, but usually brings about steric hindrance and induces nonspecific interactions, inhibiting the specific recognition by biomolecules. Additionally, a larger molecular size upon bis-labeling probably inhibits the cellular internalization. Bioorthogonal chemistry is a powerful method that has been used for labeling biomolecules in their native environments. In this work, we demonstrated intracellular bis-labeling of a phosphorescent iridium(III) complex and a fluorescent rhodamine derivative via two bioorthogonal reactions onto the tetrapeptide DEVD, which is a substrate of the cutting enzyme caspase-3, affording an FRET-based sensor for the catalytic activity of caspase-3 during cellular apoptosis. Owing to the high specificity, the two labeling processes did not interfere with each other even in the intracellular environment. Experimental detection and computational molecular docking showed that the bis-labeling of the donor/acceptor pair reduced the specificity and affinity of the DEVD-caspase-3 recognition. To address this issue, we designed a new “labeling after recognition” sensing approach, in which bioorthogonal labeling occurred after the substrate was recognized and cleaved by caspase-3. In real-time long-term cellular imaging, the photoluminescence intensity was interfered by dynamic concentration variation of the luminophores in living cells. We used PLIM to measure photoluminescence lifetimes as a sensitive indicator for caspase-3. Compared to traditional “labeling before recognition” sensing and imaging, the sensitivity in the new “labeling after recognition” approach was remarkably improved because the steric hindrance and/or non-specific interaction was minimized. Lifetime analysis also gave more information on the catalytic peptide cleavage compared to the intensity-based imaging. Analysis the relative occurrence of long-lived and short-lived signals in the images gave an approximate idea about the extent to which the catalytic cleavage occurred. This new sensing approach involving intracellular bioorthogonal labeling, “labeling after recognition”, and photoluminescence lifetime imaging can be easily and widely used for imaging other cutting enzymes or biomolecules in living cells during specific cellular activities. In the future, with the fast development of bioorthogonal chemistry and the photoluminescence lifetime imaging technique, “labeling after recognition” represents a new powerful platform for the non-invasive detection and imaging of biological activities.

## ASSOCIATED CONTENT

**Supporting Information.** Synthesis, characterization, experimental information, and additional figures. This material is available free of charge via the Internet at <http://pubs.acs.org>.

## AUTHOR INFORMATION

### Corresponding Author

\*iamy Zhang@njupt.edu.cn

\*iamqzhao@njupt.edu.cn

\*wei-huang@njtech.edu.cn.

### Notes

The authors declare no competing financial interest.

## ACKNOWLEDGMENT

We thank National Funds for Distinguished Young Scientists (61825503), National Natural Science Foundation of China (61975085), Natural Science Foundation of Jiangsu Province of China (BK20190088), Nanjing University of Posts and Telecommunications (NY218159) for financial support. Q.W. acknowledges the receipt of Postgraduate Research & Practice Innovation Program of Jiangsu Province (46030CX18036). K.Y.Z. acknowledges the receipt of Qing Lan Project of Jiangsu Province and 1311 Project of Nanjing University of Posts and Telecommunications.

## REFERENCES

- (1) Dagher, M.; Kleinman, M.; Ng, A.; Juncker D. Ensemble Multicolour FRET Model Enables Barcoding at Extreme FRET Levels. *Nature Nanotech.* **2018**, *13*, 925–932.
- (2) Hellenkamp, B.; Schmid, S.; Doroshenko, O.; Opanasyuk, O.; Kühnemuth, R.; Adariani, S. R.; Ambrose, B.; Aznauryan, M.; Barth, A.; Birkedal, V.; Bowen, M. E.; Chen, H. T.; Cordes, T.; Eilert, T.; Fijen, C.; Gebhardt, C.; Götz, M.; Gouridis, G.; Gratton, E.; Ha, T.; Hao, P. Y.; Hanke, C. A.; Hartmann, A.; Hendrix, J.; Hildebrandt, L. L.; Hirschfeld, V.; Hohlbein, J.; Hua, B. Y.; Hübler, C. G.; Eleni Kallis, Kapanidis, A. N.; Kim, J.-Y.; Krainer, G.; Lamb, D. C.; Lee, N. K.; Lemke, E. A.; Levesque, B.; Levitus, M.; McCann, J. J.; Naredi-Rainer, N.; Nettels, D.; Ngo, T.; Qiu, R. Y.; Robb, N. C.; Röcker, C.; Sanabria, H.; Schlierf, M.; Schröder, T.; Schuler, B.; Seidel, H.; Streit, L.; Thurn, J.; Tinnefeld, P.; Tyagi, S.; Vandenberk, N.; Manuel Vera, A.; Weninger, K. R.; Wunsch, B.; Yanez-Orozco, I. S.; Michaelis, J.; Seidel, C. A. M.; Craggs, T. D.; Hugel, T. Precision and Accuracy of Single-Molecule FRET Measurements—a Multi-laboratory Benchmark Study. *Nat. Methods* **2018**, *15*, 669–676.
- (3) Algar, W. R.; Hildebrandt, N.; Vogel, S. S.; Medintz, I. L. FRET as a Biomolecular Research Tool—Understanding Its Potential While Avoiding Pitfalls. *Nat. Methods* **2019**, *16*, 815–829.
- (4) Marx, V. Probes: FRET Sensor Design and Optimization. *Nat. Methods* **2017**, *14*, 949–953.
- (5) Reddy G, U.; A, A. H.; Ali, F.; Taye, N.; Chattopadhyay, S.; Das, A. FRET-Based Probe for Monitoring pH Changes in Lipid-Dense Region of Hct116 Cells. *Org. Lett.* **2015**, *17*, 5532–5535.
- (6) Chung, C. Y.-S.; Posimo, J. M.; Lee, S.; Tsang, T.; Davis, J. M.; Brady, D. C.; Chang, C. J. Activity-Based Ratiometric FRET Probe Reveals Oncogene-Driven Changes in Labile Copper Pools Induced by Altered Glutathione Metabolism. *Proc. Natl. Acad. Sci. U.S.A.* **2019**, *116*, 18285–18294.
- (7) Aron, A. T.; Loehr, M. O.; Bogena, J.; Chang, C. J. An Endoperoxide Reactivity-Based FRET Probe for Ratiometric Fluorescence Imaging of Labile Iron Pools in Living Cells. *J. Am. Chem. Soc.* **2016**, *138*, 14338–14346.
- (8) Zhao, Q.; Huo, F.; Kang, J.; Zhang, Y.; Yin, C. A Novel FRET-Based Fluorescent Probe for the Selective Detection of Hydrogen Sulfide ( $\text{H}_2\text{S}$ ) and Its Application for Bioimaging. *J. Mater. Chem. B.* **2018**, *6*, 4903–4908.
- (9) Su, D.; Teoh, C. L.; Sahu, S.; Das, R. K.; Chang, Y.-T. Live Cells Imaging Using A Turn-On FRET-Based BODIPY Probe for Biothiols. *Biomaterials* **2014**, *35*, 6078–6085.
- (10) Ma, Y.; Yamamoto, Y.; Nicovich, P. R.; Goyette, J.; Rossy, J.; Gooding, J. J.; Gaus, K. A FRET Sensor Enables Quantitative

Measurements of Membrane Charges in Live Cells. *Nat. Biotechnol.* **2017**, *35*, 363–370.

(11) Dyla, M.; Terry, D. S.; Kjaergaard, M.; Sørensen, T. L.-M.; Andersen, J. L.; Andersen, J. P.; Knudsen, C. R.; Altman, R. B.; Nissen, P.; Blanchard, S. C. Dynamics of P-Type ATPase Transport Revealed by Single-Molecule FRET. *Nature* **2017**, *551*, 346–351.

(12) Murai, S.; Yamaguchi, Y.; Shirasaki, Y.; Yamagishi, M.; Shindo, R.; Hildebrand, J. M.; Miura, R.; Nakabayashi, O.; Totsuka, M.; Tomida, T.; Adachi-Akahane, S.; Uemura, S.; Silke, J.; Yagita, H.; Miura, M.; Nakano, H. A FRET Biosensor for Necroptosis Uncovers Two Different Modes of the Release of DAMPs. *Nat. Commun.* **2018**, *9*, 4457.

(13) Mu, J.; Liu, F.; Rajab, M. S.; Shi, M.; Li, S.; Goh, C.; Lu L.; Xu, Q.-H.; Liu, B.; Ng, L. G.; Xing, B. G. A Small-Molecule FRET Reporter for the Real-Time Visualization of Cell-Surface Proteolytic Enzyme Functions. *Angew. Chem. Int. Ed.* **2014**, *53*, 14357–14362.

(14) Pinkert, T.; Furkert, D.; Korte, T.; Herrmann, A.; Arenz, C. Amplification of a FRET Probe by Lipid-Water Partition for the Detection of Acid Sphingomyelinase in Live Cells. *Angew. Chem. Int. Ed.* **2017**, *56*, 2790–2794.

(15) Prescher, J. A.; Bertozzi, C. R. Chemistry in Living Systems. *Nat. Chem. Biol.* **2005**, *1*, 13–21.

(16) Boyce, M.; Bertozzi, C. R. Bringing Chemistry to Life. *Nat. Methods* **2011**, *8*, 638–642.

(17) Yuan, L.; Lin, W.; Zheng, K.; Zhu, FRET-Based Small-Molecule Fluorescent Probes: Rational Design and Bioimaging Applications. *S. Acc. Chem. Res.* **2013**, *46*, 1462–1473.

(18) Row, R. D.; Prescher, J. Constructing New Bioorthogonal Reagents and Reactions. *A. Acc. Chem. Res.* **2018**, *51*, 1073–1081.

(19) Liang, Y.; Mackey, J. L.; Lopez, S. A.; Liu, F.; Houk, K. N. Control and Design of Mutual Orthogonality in Bioorthogonal Cycloadditions. *J. Am. Chem. Soc.* **2012**, *134*, 17904–17907.

(20) Li, B.; Zhou, X.-H.; Yang, P.-Y.; Zhu, L. P.; Zhong, Y.; Cai, Z. J.; Jiang, B.; Cai, X. Q.; Liu, J.; Jiang, X. X. Photoactivatable Fluorogenic Labeling via Turn-On “Click-Like” Nitroso-Diene Bioorthogonal Reaction. *Adv. Sci.* **2019**, *6*, 1802039.

(21) Lee, L. C.-C.; Lau, J. C.-W.; Liu, H.-W.; Lo, K. K.-W. Conferring Phosphorogenic Properties on Iridium(III)-Based Bioorthogonal Probes through Modification with a Nitron Unit. *Angew. Chem. Int. Ed.* **2016**, *55*, 1046–1049.

(22) Wang, J.; Xue, J.; Yan, Z.; Zhang, S.; Qiao, J.; Zhang, X. Photoluminescence Lifetime Imaging of Synthesized Proteins in Living Cells Using an Iridium-Alkyne Probe. *Angew. Chem. Int. Ed.* **2017**, *56*, 14928–14932.

(23) Yang, F.; Gao, H.; Li, S.-S.; An, R.-B.; Sun, X.-Y.; Kang, B.; Xu, J.-J.; Chen, H.-Y. A Fluorescent  $\tau$ -Probe: Quantitative Imaging of Ultra-Trace Endogenous Hydrogen Polysulfide in Cells and in Vivo. *Chem. Sci.* **2018**, *9*, 5556–5563.

(24) Gopich, I. V.; Szabo, A. Theory of the Energy Transfer Efficiency and Fluorescence Lifetime Distribution in Single-Molecule FRET. *Proc. Natl. Acad. Sci. U.S.A.* **2012**, *109*, 7747–7752.

(25) Zhang, K. Y.; Yu, Q.; Wei, H. J.; Liu, S. J.; Zhao, Q.; Huang, W. Long-Lived Emissive Probes for Time-Resolved Photoluminescence Bioimaging and Biosensing. *Chem. Rev.* **2018**, *118*, 1770–1839.

(26) Rossé, T.; Olivier, R.; Monney, L.; Rager, M.; Conus, S.; Fellay, I.; Jansen, B.; Borner, C. Bcl-2 Prolongs Cell Survival after Bax-Induced Release of Cytochrome *c*. *Nature* **1998**, *391*, 496–499.

(27) Dommerholt, J.; Rooijen, O.; Borrmann, A.; Guerra, C. F.; Bickelhaupt, F. M.; van Delft, F. L. Highly Accelerated Inverse Electron-Demand Cycloaddition of Electron-Deficient Azides with Aliphatic Cyclooctynes. *Nat. Commun.* **2014**, *5*, 5378.

(28) Tang, T. S.-M.; Yip, A. M.-H.; Zhang, K. Y.; Liu, H.-W.; Wu, P. L.; Li, K. F.; Cheah, K. W.; Lo, K. K.-W. Bioorthogonal Labeling, Bioimaging, and Photocytotoxicity Studies of Phosphorescent Ruthenium(II) Polypyridine Dibenzocyclooctyne Complexes. *Chem. Eur. J.* **2015**, *21*, 10729–10740.

(29) Lo, K. K.-W.; Chan, B. T.-N.; Liu, H.-W.; Zhang, K. Y.; Li, S. P.-Y.; Tang, T. S.-M. Cyclometalated Iridium(III) Polypyridine

Dibenzocyclooctyne Complexes as the First Phosphorescent Bioorthogonal Probes. *Chem. Commun.* **2013**, *49*, 4271–4273.

(30) Choi, A. W.-T.; Liu, H.-W.; Lo, K. K.-W. Ruthenium(I) Polypyridine Dibenzocyclooctyne Complexes as Phosphorescent Bioorthogonal Probes: Synthesis, Characterization, Emissive Behavior, and Biolabeling Properties. *J. Inorg. Biochem.* **2015**, *148*, 2–10.

(31) Liang, Y.; Jiang, X.; Yuan, R.; Zhou, Y.; Ji, C.; Yang, L.; Chen, H.; Wang, Q. Metabolism-Based Click-Mediated Platform for Specific Imaging and Quantification of Cell Surface Sialic Acids. *Anal. Chem.* **2017**, *89*, 538–543.

(32) Wu, H. X.; Devaraj, N. K. Advances in Tetrazine Bioorthogonal Chemistry Driven by the Synthesis of Novel Tetrazines and Dienophiles. *Acc. Chem. Res.* **2018**, *51*, 1249–1259.

(33) London, N.; Miller, R. M.; Krishnan, S.; Uchida, K.; Irwin, J. J.; Eidam, O.; Gibold, L.; Cimermančič, P.; Bonnet, R.; Shoichet, B. K.; Taunton, J. Covalent Docking of Large Libraries for the Discovery of Chemical Probes. *Nat. Chem. Biol.* **2014**, *10*, 1066–1072.

(34) Zhang, Y.; Sanner, M. F. Docking Flexible Cyclic Peptides with *AutoDock CrankPep*. *J. Chem. Theory Comput.* **2019**, *15*, 5161–5168.

(35) Shraga, A.; Olshvang, E.; Davidzohn, N.; Khoshkenar, P.; Germain, N.; Shurrush, K.; Carvalho, S.; Avram, L.; Albeck, S.; Unger, T.; Lefker, B.; Subramanyam, C.; Hudkins, R. L.; Mitchell, A.; Shulman, Z.; Kinoshita, T.; London, N. Covalent Docking Identifies a Potent and Selective MKK7 Inhibitor. *Cell Chem. Biol.* **2019**, *26*, 98–108.

(36) Berman, H. M.; Westbrook, J.; Feng, Z.; Gilliland, G.; Bhat, T. N.; Weissig, H.; Shindyalov, I. N.; Bourne, P. E. The Protein Data Bank. *Nucleic Acids Res.* **2000**, *28*, 235–242.

(37) Chang, Y.-J.; Linh, N. H.; Shih, Y. H.; Yu, H.-M.; Li, M. S.; Chen, Y.-R. Alzheimer's Amyloid- $\beta$  Sequesters Caspase-3 in Vitro via Its C-Terminal Tail. *ACS Chem. Neurosci.* **2016**, *7*, 1097–1106.

(38) Scarpino, A.; Ferency, G. G.; Keserü, G. M. Comparative Evaluation of Covalent Docking Tools. *J. Chem. Inf. Model.* **2018**, *58*, 1441–1458.

(39) Zeng, W.; Du, Z.; Luo, Q.; Zhao, Y.; Wang, Y.; Wu, K.; Jia, F.; Zhang, Y.; Wang, F. Proteomic Strategy for Identification of Proteins Responding to Cisplatin-Damaged DNA. *Anal. Chem.* **2019**, *91*, 6035–6042.

(40) Li, F.-L.; Liu, J.-P.; Bao, R.-P.; Yan, G. Q.; Feng, X.; Xu, Y.-P.; Sun, Y.-P.; Yan, W. L.; Ling, Z.-Q.; Xiong, Y.; Guan, K.-L.; Yuan, H.-X. Acetylation Accumulates PFKFB3 in Cytoplasm to Promote Glycolysis and Protects Cells from Cisplatin-Induced Apoptosis. *Nat. Commun.* **2018**, *9*, 508.

## Table of Contents artwork

